Accepted Manuscript

CMAS Corrosion of EB PVD TBCs: Identifying the Minimum Level to Initiate Damage

R. Wellman, G. Whitman, J.R. Nicholls
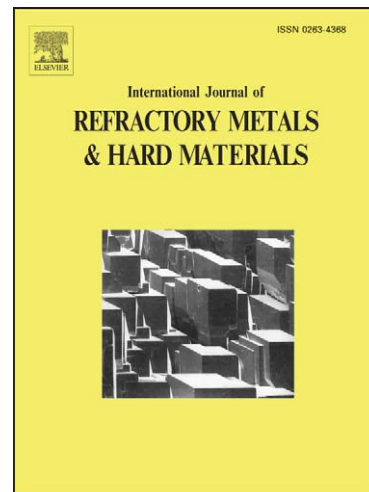
Please cite this article as: Wellman, R., Whitman, G., Nicholls, J.R., CMAS Corrosion of EB PVD TBCs: Identifying the Minimum Level to Initiate Damage, *International Journal of Refractory Metals & Hard Materials* (2009), doi: 10.1016/j.ijrmhm.2009.07.005

CMAS Corrosion of EB PVD TBCs: Identifying the Minimum Level to Initiate Damage

R. Wellman, G. Whitman and J. R. Nicholls

National High Temperature Surface Engineering Centre, Cranfield University, UK

Over the last decade a significant amount of research has been conducted into the durability of thermal barrier coatings (TBCs) focusing mainly on issues of oxidation, erosion and Foreign Object Damage (FOD). However, as the performance and durability of TBCs has improved the temperatures at which they operate has increased.   This increase in temperature has resulted in another lifing issue for EB-PVD TBCs, namely that of CMAS attack.   Calcium magnesium alumino-silicate (CMAS) attack occurs when atmospheric dust that has deposited on the surface of turbine blades melts and wicks into the columns of the TBC.   This occurs at temperatures above 1240-1260°C and results in the degradation of the columnar microstructure of the TBCs. Due to the fact that TBCs operate in a temperature gradient CMAS only infiltrates part of the coating before solidifying.

There are a number of issues associated with CMAS attack, both chemical and mechanical. From a chemical point of view CMAS attack of Electron Beam (EB) Physical Vapour Deposited (PVD) TBCs can be considered as a form of corrosion; when there is a lot of excess CMAS on the surface of a coated component Yttria diffuses out of the TBC into the molten CMAS resulting in a t' to monoclinic phase transformation in the Yttria Stabilised Zirconia (YSZ), CMAS attack also results in localised melting and subsequent re-precipitation of the coating resulting in a loss of the defined columnar microstructure.   While from a mechanical point of view the CMAS, once re-solidified, reduces the strain compliance of the EB-PVD and can result in spallation of the TBC on cooling. Furthermore, current studies have indicated that small amounts of CMAS infiltration significantly increases the erosion rate of EB-PVD TBCs.

This paper covers various aspects of CMAS attack of EB-PVD TBCs, specifically looking at minimum levels of CMAS required to initiate damage, as well as investigating it from an erosion-corrosion perspective.

Keywords: EB PVD TBC, CMAS, Degradation, Erosion

1. Introduction

Thermal Barrier Coatings are used to limit the heat transfer through a coating and to protect vital engine components from oxidation and hot corrosion. A TBC system generally consists of three layers and outer YSZ ceramic layer typically 125-200µm thick which is applied to a thin alumina layer, the TGO, (initially this is in the order of 1µm thick) which forms on the bond coat. The bond coat is typically either a Pt-aluminide or and MCrAly layer.

One of the primary causes of failure of TBCs has been attributed to oxidation of the bond coat and growth of the Thermally Grown Oxide (TGO) [1]. Erosion has been named as the second most common failure mode, caused by the ingestion of particles, which leads to thinning of the TBC, reducing insulation and increasing the TGO growth rate [1].

Increasing turbine inlet temperature has seen a rapid increase in corrosion problems caused by molten deposits, otherwise known as calcium-magnesium-alumino-silicate (CMAS) attack.   The porous structure of EB PVD TBCs makes it susceptible to this type of attack, with the CMAS infiltrating the pores and column boundaries resulting in both chemical and micro structural degradation of the coating [2]. As there is a large coefficient of thermal expansion mismatch between the CMAS and the TBC, the added stain energy stored in the CMAS can lead to delamination and spalling between the TBC and bond coat [3].

In 1992, Kim et al identified problems associated with the deposition of volcanic materials onto the hot sections of gas turbines [4]. Although this work did not involve components with TBCs, it did

serve to identify degradation due to blockage and cooling of molten deposits leading to further studies in this area. By injecting known amounts of volcanic ash into the hot sections, it was identified that the composition melted between 1090 and 1150°C, whereby the deposit became molten and adhered to surfaces. Further research extended to more modern engines showed that TBC degradation occurred when engines ingested particles and other debris in sandy middle eastern environments, which also became molten and adhered to the surface of TBC coated components, but only when temperatures exceeded 1150°C [5]. It was suggested that these molten deposits led to an increase in coating stress due to the thermal expansion mismatch, causing spallation of the TBC. Penetration of CMAS into pores is said to result in the loss of strain tolerance, leading to progressive exfoliation of the coating on thermal cycles.

Scott et al specifically investigated TBC performance on jet engines, which were used in the Middle East, where these molten deposits were first identified as CMAS [6]. A common observation across all literature was that compositions of mineral intake were similar and all contained CaO, MgO, Al_2O_3 and SiO_2. This means that the correct components for CMAS are present in generic 'dirt' and that only the ratios of these components differ. When these constituents come together in the correct composition range then it forms the low melting point eutectic Calcium-magnesium-alumino-silicate (CMAS). Depending on the composition of CMAS the melting point is usually approximately 1240°C, much lower than the melting point of the constituents which by themselves would not cause a problem.

It was observed that very fine particles, with a diameter less than 10 microns can pass through the particle separators and enter the combustor systems. Usually, these particles do not possess sufficient kinetic energy to cause impact damage to the TBC, however they are aerodynamically captured within the combustor gases (due to the leading edge and pressure surface of the aerofoil) and deposit onto the surface [3].

Work by Borom, who investigated the spallation of Air Plasma Sprayed TBCs [5] showed that spallation was linked to the infiltration of molten deposits. An important observation was that, from all available oxides in external environments, only CaO, MgO, Al_2O_3 and SiO_2 made up the molten phase that penetrated into the TBC microstructure. Most elements in the earths crust and soil occur in minerals, with oxygen, silicon, aluminium, iron, magnesium and calcium being the most common chemical elements [7], giving the scope for CMAS formation in a wide range of locations. It is due to the abundance of these elements in nature that leads to the easy deposition of the constituents of CMAS into engines, leading to significant corrosion problems. Many of these materials are transported into the soils and atmosphere in volcanic plumes [8].

Dolomite, which is a calcium magnesium carbonate, has been identified as the most common component found in the gas path in Saudi Arabia, and was associated with the degradation of engine performance. Dolomite would only need to combine in small amount with an aluminosilicate, which are also abundant within the same regions, to readily form CMAS within a gas turbine. Many of these minerals named above have been identified in the locations where CMAS attack presents a large problem to aircraft. Any combination of the above minerals when present and in the correct composition will combine leading to significant corrosion problems.

CMAS is said to attack as a 'moving front', first by becoming molten and infiltrating into the TBC pores. When the CMAS cools, it freezes, locking together columns tips and the coating loses it ability to accommodate strains due to the thermal expansion mismatch with the super alloy base metal. It follows that the coating will suffer delamination cracking leading to the progressive exfoliation of discrete layers or spallation of the TBC coating, leading to the loss of thermal efficiency and degradation of the base metal component. Simultaneously, the coating has been reported to undergo severe chemical attack from the CMAS [9].

Research by Stott et al was one of the first studies to show that TBC coatings were degraded readily by the molten sands and molten glass debris [6]. It was claimed that the zirconia and yttria were

absorbed from the ceramic during attack that happened preferentially at grain boundaries. It was noted that when the solubility limit of the Zirconia was exceeded that the phase was reprociprated as a monoclinic fine grain structure depleted in yttria. This has also been reported in other studies; Kramer in particular has studied the effects of CMAS attack in great depth [9-12] and found that CMAS rapidly penetrates the open structure of an EB PVD TBC upon melting, which leads to changes in chemistry and microstructure. The original YSZ is said to dissolve in CMAS and re-precipitate with a different morphology and composition. The extent of penetration is controlled by the interaction between the thermal gradient through the TBC with the fluidity of the melt. They also observed that the CMAS composition did not melt, penetrate or adhere to the substrate at temperatures below 1230°C, partial melting was observed at 1235°C which was completed by 1240°C.

CMAS was observed to penetrate right down to the substrate, noticeably attacking the alumina TGO, which promoted detachment of the TBC. The failure mechanism was identified as the infiltration of CMAS between the intercolumnar pores, resulting in a monolith structure when cool with complete loss of the strain tolerance. Examination of the samples showed that the bulk of the columns remained intact but were impregnated with CMAS, whereas the column tips, (columns / bulk CMAS interface) and substrate / TBC interface showed significant degradation, as shown in Figure 1.

Kramer observed that the column tips completely lost their identity, and were replaced with a series of globular particles that were embedded with CMAS. The effect of temperature of this 'upper' reaction zone was that the area of degradation increased with increasing temperature significantly. At 1240°C, the area of globular particles extended just 14μm into the coating, but by 1400°C this had extended to approximately 42μm. However, with that said, it was noted that the general appearance of the degraded area was not related to temperature, and the 'number' of globular particles did not increase with increased temperature.

All open capillaries in any TBC structure are vulnerable to CMAS attack due to its excellent wetting properties, particularly on YSZ, and it is able to spread rapidly over the surface and penetrate the structure. Infiltration rate is affected by the availability of the melt; hence melt kinetics [12], as well as capillary-driven flow into a porous medium [9].

From calculations, Kramer estimated that the infiltration of a 200μm EB-PVD TBC coating took less than one minute, even at the lowest recorded melting temperature of 1240°C [9]. It is therefore expected that the CMAS is able to infiltrate a coating from tips to the substrate even before the highest temperature has been reached, explaining why the attack of the substrate / TBC interface occurs at temperatures just above melting temperatures.

The maximum operating temperature of TBCs is potentially being limited by CMAS infiltration. When this deposit melts, it is drawn by a capillary action into all open pores due to the morphology and structure of the TBC. When the temperature is reduced, the CMAS cools and solidifies, resulting in the infiltrated area developing a high modulus [11]. With the whole penetrated region essentially being a solid structure, there is a complete loss of strain tolerance as well as a decrease in thermal conductivity. It is when the CMAS infiltrated region is subject to rapid cooling that delamination becomes the dominant form of failure. This loss of strain tolerance is a significant problem with TBCs as it makes them susceptible to thermomechanical failure brought about by the thermal cycling experienced by TBCs during their normal operations.

Both EB-PVD and APS TBCs are susceptible to loss of strain tolerance, due to the porous structures, which are designed specifically to be effective in reducing thermal conductivity as well as accommodating the thermal expansion mismatch between the TBC and substrate. Once the CMAS cools sufficiently the TBC becomes a fully dense domain, locking together the tips of the columns and splats, the thermal expansion mismatch causes crack initiation and propagation ultimately leading to the complete loss of the TBC.

With delamination and spalling identified as the most prominent form of failure attributed to CMAS, there is a wide range of literature on this aspect when compared to the thermochemical mechanism. Mercer, in 2004, investigated delamination mechanisms for EB-PVD TBCs that were subject to CMAS infiltration, which he associated with 'cold shock' on engine shut down [11]. He identified that there were potentially three important mechanisms, in which he based upon observation of the sub-surface delamination within infiltrated regions. Using these observations he made the following assumptions: "a) The sub-surface delamination always infiltrates at surface-connected vertical separation, b) They are fully infiltrated with CMAS, and c) they are strictly mode I" [11].

Figure 2 is an example of delaminations that occur on both TBCs on aerofoils and shrouds, and is in agreement with statements made by Mercer [11] and Chen [13], that delaminations occur in mode I and always extend from surface cracks.

Finally, recommendations concerning the critical penetration depth that causes cold shock delaminations showed that this thickness is dependant upon heat transfer coefficient. This implies that there is a heat transfer coefficient below which delamination can be avoided. A rapid shock model created using shock analysis predicted that the critical infiltration thickness is approximately 30μm, although for less severe shocks this thickness would be larger. Using this model Mercer has suggested two possible techniques for the prevention of this delamination mechanism, this includes maintaining the temperature at a range that ensures the CMAS infiltration depth is kept below this critical thickness. This other method is to control the critical cooling rate during engine shut down.

It was found from investigating components used in the field that the depth of penetration of the CMAS is location dependant. The depth of penetration had a significant impact on the delamination, with the deeply infiltrated regions exhibiting multiple sub-surface delaminations which originate from a single channel crack. The location of the delaminations were found to predominate at three levels, those being, just above the bond coat, adjacent to the bottom of the CMAS infiltrated area and just below the top surface, with the most important of these being shown in figure 14.

Delaminations just below the top surface were found to be completely filled with CMAS, hence usually still firmly adhered. Those adjacent to the bottom of the CMAS infiltrated area tended to link together, causing large sections to spall, in what was described as a "slab of ejected material". Those just above the bond coat were found to be the most detrimental to the durability of the coating as they were usually extremely long.

The CMAS composition with depth into the TBC varied, with shows that there are a series of melting and infiltration steps that are "consistent with the stochastic nature of the ingestion and deposition of siliceous debris" [14]. Using TEM Kramer ascertained that the CMAS structure itself changed at a depth of 150μm. At the surface of the examined component the structure of the CMAS is amorphous, and as it penetrates deeper into the coating it became crystalline. Large globular particles were identified at 180μm in depth and were identified as re-precipitated zirconia, which suggests that the CMAS crystallises after dissolution. It probably should be noted that there was no mention of the temperatures that the shrouds were subject to during this study, which makes comparison of this research to other studies rather difficult, as it is highly likely that the severity of any CMAS attack is dependant upon the temperature. It is also likely that the temperature experienced by this component varied greatly during operation, hence depending upon where the component was section was likely to give a different solution.

It is evident from the literature that CMAS attack of EB PVD TBCs is starting to become a lifing issue for some turbine engines, and is being investigated, however, most of the research either uses engine run components or samples which have large amounts of CMAS deposited onto the coating. This paper is the first to investigate the minimum levels of CMAS deposition required to initiate CMAS attack. Another issue which has not yet been resolved is when the CMAS is formed. Does atmospheric dust react in the combustor to form CMAS which then deposits onto the turbine blades? Or do the various constituent powders deposit onto the turbine blades and then form CMAS if / when

the surface temperature of the blade exceeds 1240°C. One of the aims of this paper was to determine the minimum level of CMAS required to initiate damage in the TBC. The reason for trying to determine the minimum levels required for attack was to be able to produce samples, for erosion testing, which were only partially infiltrated with CMAS and thus determine the effect of CMAS attack on the erosion of EB PVD TBC, in other words to determine the erosion-corrosion behaviour of EB PVD TBCs.

2. Test Method

In order to establish the minimum level of CMAS required to infiltrate and attack a TBC, small levels of CMAS and powders were sprayed (in a water suspension) onto EB PVD TBCs and then heat treated at 1300°C for 4hrs to ensure that there was sufficient time for CMAS attack to occur. To this end EB PVD TBC samples which had been deposited onto single crystal pure (99.99%) alumina were coated with 0.0075g, 0.01g, 0.015g 0.02g and 0.03g of CMAS powder and heat treated.

Due to the fact that all the heat treatments were conducted (in air) in a tube furnace under isothermal conditions 99.99% purity sapphire discs were used as the substrates for EB PVD TBC deposition. Only one composition of CMAS was used in this study, 48 SiO2 - 35CaO – 10MgO – 7Al$_2$O$_3$(mol%), although it was used in two different forms, as a chemically reacted CMAS and as the component powders referred to as reacted CMAS and constituent powders in this paper.

To deposit the CMAS a spray gun method was adopted in order to ensure the most uniform and accurate coverage possible. The spraying was carried out within a fume cupboard, which contained a heated plate, a clamp and the spray gun. The spray gun was externally connected to a compressed air line, and held in the clamp to ensure it was always in the same position when spraying the sample.

All heat treatment took place in a horizontal tubular Al$_2$O$_3$ furnace. This furnace is controlled electronically and has a maximum operating temperature of 1500°C. Samples were loaded onto Al$_2$O$_3$ 'boats', which were pushed into the working section of the furnace.

The hot target was set to the temperature required, in most cases this was 1300°C with a ramp up time of 10°C/min. The dwell time was set in minutes to the length required before the furnace was set to ramp down to 20°C, which was also set at 10°C/min. During all of these heat treatments the furnace was never loaded or unloaded when the furnace was hot, and in all experiments the samples were removed when the furnace temperature gauge read room temperature.

3. Results

3.1 Initial CMAS Investigation

The first samples to be examined were those that were subject to large quantities of CMAS (120mg/cm^2) in order to establish if degradation occurred at the chosen CMAS composition and conditions. On removal from the furnace, both types of CMAS samples appeared to have a glassy texture on the surface.

CMAS1, the compressed and heat-treated 'reacted' CMAS shown in Figure 3(a), showed no damage to the TBC, and had a thick glassy coating of CMAS. CMAS2, made solely from the constituent powders also had a thick CMAS coating, but the TBC had several large cracks, shown in Figure 3(b).

In order to establish whether the level of attack on these two samples was the same, both samples were examined using Raman Spectroscopy and ESEM.

The samples were examined in cross section using Raman Spectroscopy, a standard 7YSZ coating with a meta stable tetragonal (t') crystal structure has characteristic peaks at 250 R cm^{-1} and 625 R

cm^{-1}. The monoclinic (m) on the other hand has a series of peaks in the 175 R cm^{-1} range with smaller peaks at between 290 to 390 R cm^{-1}.

Figure 4 shows the Raman Spectrum for samples CMAS1 and CMAS2 compared with the standard 7YSZ. This confirms that at high levels of CMAS deposition there is a shift from tetragonal to monoclinic, although there was not a complete transformation. It is also interesting to note that the constituent powder (CMAS2) has shifted considerably more towards monoclinic than the reacted CMAS (CMAS1).

Raman spectroscopy revealed that the constituent powders appeared to have a more pronounced shift towards monoclinic than reacted CMAS, which is the first indication that the different types may not be having the same effect. In order to show whether the two CMAS types were equivalent the samples were examined using the Environmental Scanning Electron Microscope, to study any changes in morphology. This equipment was also used to study the composition and look for changes to the TBC using elemental analysis (EDX), which could be used to explain why a difference in the Raman spectra was observed.

The results showed almost identical damage to the TBC structure with both CMAS types, see Figure 6. The damage occurred in terms of severe damage to the tips of the TBC columns, and at first glance both appear to be full of holes. Elemental analyses of the 'holes' (dark regions) showed that they have the same composition as the bulk CMAS, with the addition of both yttria and zirconia and shows how CMAS has infiltrated and solidified within the columns.

Elemental analysis confirmed that the tips of the columns are depleted in yttria when the CMAS degraded samples were compared with the control, showing a drop of approximately one third, which is in agreement with previous research by Kramer [9].

3.2 Determination of Minimum Level Required for CMAS Attack

The ESEM was used to examine the cross sections of the samples subjected to CMAS attack concentrating on the tips of the columns and the TBC substrate interface. These were then compared to a reference sample shown in Figure 7. The Micrographs in figures 7 to 9 are all of fracture sections.

In order to assess the damage from the CMAS, closer examination of the samples which had constituent powder CMAS applied were examined, starting from the sample that had received the lowest amount, 0.0075g (1.8mg/cm^2).

It can be seen from these images that the columns and column tips remain intact, with very little difference between the images in Figure 8 and the control shown in Figure 7. From the lower magnification image there appears to be evidence of very minimal CMAS attack, however the TBC still appears to be fully adhered to the substrate from closer examination of the interface. From these images it can be assumed from the good adherence and very minimal damage to the intracolunmar structure that 1.8mg/cm^2 is a safe level of CMAS attack.

Following this samples that had increasing amounts of CMAS (0.01g, 0.0125g, 0.02g and 0.03g) were examined after heat treatment for 4hrs at 1300°C.

In the sample with 0.01g, CMAS degradation to the column tips was beginning to initiate, with the damage only affecting column tips sporadically across the surface with a number of areas that remained completely unaffected. This was common across the entire surface of the sample. It could be assumed that the sporadic degradation was a consequence of 'non-uniform' coverage of the CMAS due to a low level being applied.

The sample with 0.0125g (3mg/cm^2) of CMAS showed little change from the 0.01g sample. Although still sporadic, there was a more distributed attack across the sample surface. There were very few

columns that were completely unaffected by the CMAS, and the formation of globular particles was becoming more apparent. The main difference between this sample and the previous was the beginning of the loss of the column tips; however this only occurred in the more severely damaged columns.

As can be seen in the SEM micrographs in Figure 10, the formation of globular particles was more consistent at this level, with nearly all columns showing evidence of CMAS attack. Many of the columns were losing their identity at the tips and it is clear that this level would have a significantly detrimental effect on the TBCs' performance. At this level the CMAS has caused degradation to a depth of approximately 30μm, which increases to 50μm in the more heavily affected areas. Again, this is a sign of non-uniform deposition, but it is clear that the CMAS attack is significant at this level.

The TBC was also examined from the top, to provide information regarding the shape of the formation of globular particles, Figure 11 shows the top of sample P_0.02, after four hours at 1300°C. As deposited, the particles would be expected to be angular and if they melt completely then surface tension would make them take on the appearance of spherical or globular particles. This is important, as the shape they produce shows if they start to wet the column tops. At temperatures just below the melting point, surface diffusion can lead to facetted crystals forming with slightly rounded edges. Hence inspection of these particles shows whether there is any interaction with ZrO_2 (Y_2O_3) and whether they have melted.

When shown next to the control in Figure 12 the image in Figure 11 shows sintering of the columns and loss of the column tips. It also shows how the sintering has occurred in patches, and only affects areas of columns rather than being distributed uniformly across the surface.

All samples were furnace cooled, i.e. cooled slowly into a near equilibrium structure of the reaction products. The shapes and sizes of the globular particles were compared with the shape and size of the constituent particles. It was found that overall, the size of the globules were smaller than the 'as deposited' particles in both types of CMAS used. The shape of the deposited particles was angular, and due to them melting completely they become more spherical and globular due to surface tension. This contact appearance provides information on surface energy, and shows that the particles wet the 7YSZ column tops, showing that there is an interaction between the CMAS and the TBC. Examination of the interface showed that spallation was starting to occur, with significant damage.

By 0.03g the spallation had become so severe that it was not possible to examine the sample using ESEM as the coating had completely delaminated from the surface of the substrate flaking off in numerous small pieces, showing that between 0.02g and 0.03g the effect of CMAS at the substrate interface becomes significant and life limiting. However, it can be assumed that by this level significant CMAS damage has occurred and 4.8mg/cm^2 (0.02g) can be defined as an unsafe level.

3.3 Erosion Testing

CMAS has been shown to have excellent erosion properties as a glazing material, so it was important to measure the erosion properties of a sample that had been sufficiently degraded, yet did not have any excess CMAS on the surface. For this reason 4.8mg/cm^2 (0.2g) of CMAS was selected, as this level had caused formation of globular particles to approximately 35μm depth within the TBC in a uniform manner (representative of a thermal gradient), yet no excess CMAS remained on the surface. Despite 30μm being described as the critical depth required to cause delamination and spalling for a rapid shock model, for the purpose of this study it was felt more important to have a sample that had uniform degradation and the samples were not subjected to a thermal shock.

In order to carry out these tests, it was first important to ensure that the level of CMAS degradation observed in the previous samples was also observed in the erosion samples. Four samples were deposited with 0.02g of CMAS and heat treated at 1300°C for four hours. One of these samples was sectioned and examined using the ESEM, prior to the erosion testing. Having confirmed that the

degradation was consistent with what had previously been observed, two samples from the same batch were then used for erosion testing and one standard TBC as a control for comparison.

Erosion testing was carried out at room temperature at a rate of 0.54g of Al_2O_3 erodent per minute. The alumina grit size used was 90-125µm and the test was carried out at an average particle velocity of 100m/s. The samples were eroded for three minutes in thirty second intervals and were weighed after each interval. During run 5 sample P-0.02a spalled significantly and the testing was stopped for this sample.

As can be seen in Figure 13 both the CMAS degraded samples had a similar erosion rate which was significantly higher than the control sample.

Both CMAS samples have a significantly higher initial erosion rate than the control, which then reduces slightly when it settles into a steady state rate. The control by comparison has a lower initial erosion rate, which then increases after the second thirty second exposure period, although remains consistently lower than the CMAS degraded samples.
The erosion rate was calculated from the gradients of the curves, and is shown in Figure 14, which shows both an initial erosion rate, which was calculated from the first point on the curve and a steady state erosion rate calculated from the straight line section of the curve.

Depending on the impact conditions and the particle size a number of different erosion mechanisms have been identified for the erosion of EB PVD TBCs by solid particle impact [15]. Under the conditions tested in this paper the near surface cracking mechanism was expected to be the predominant mode of material loss. This was indeed found to be the case for both the control and the CMAS infiltrated samples. However, as can be seen in Figure 15b, in the control sample the columns of the TBC are discreet and cracks do not propagate into neighbouring columns. While in the samples infiltrated with CMAS the columns are no longer discreet and, as indicated by the arrows, cracks initiated in one column can propagate into other columns. This results in a higher mass loss per impact and thus a higher erosion rate.

Also of interest is the fact that the initial erosion rate of the infiltrated samples was significantly higher than the steady state erosion rate. This has been attributed to the fact that the samples were infiltrated to a depth of around 30µm and that this layer was most likely totally removed in the first erosion run. Further investigations are required to determine precisely why the infiltration of CMAS has such a significant effect on the erosion rate of the coating.

4. Conclusion

- CMAS causes severe damage to the column morphology, due to a dissolution – re-precipitation mechanism and sintering of columns. This degradation then reduces the TBCs insulating properties and reduces its strain tolerance.
- The minimum level at which CMAS degradation occurs uniformly over the column tips was found to be 4.8mg/cm^2 after 4 hours at 1300°C, hence this can be defined as the minimum level at which the TBC would start to lose its ability to protect vital engine components. Although this observation is specific for both the conditions of the tests and the composition of the CMAS used, this work has shown that minimum levels do exist although they may vary for different conditions and CMAS compositions.
- Raman spectroscopy confirms a change in crystal structure from tetragonal to monoclinic, due to depletion in yttria.
- CMAS degradation leads to a significant increase in the erosion rate of TBCs, even at the minimum level of 4.8mg/cm^2.

8. Reference

[1.] R. Wellman and J. R. Nicholls, Erosion, Corrosion and Erosion-Corrosion of EB-PVD Thermal Barrier Coatings. Tribology International 41 (2008) 657 – 662.

[2.] P. Leyen, U. Schulz, B. Pint, and I. Wright. [online]. Influence of EB-PVD TBC Microstructure on Thermal Barrier Coating System Performance under Cyclic Oxidation Conditions, (1999)   [Accessed 24th May 2008]

[3.] T. Strangman, D. Raybould, A. Jamell and W. Baker, Damage Mechanisms, Life Prediction and Development of EB-PVD Thermal Barrier Coatings for Turbine Airfoils. Surface and Coatings Technology 202, (2007) 658 – 664.

[4.] J. Kim, M. Dunn, A. Baran, D. Wade and E. Tremba, Deposition of Volcanic Materials in the hot sections of Two Gas Turbine Engines, Journal of Engineering for Gas Turbines and Power. Vol. 155 (1993) 641 - 651.

[5.] M. Borom, C. Johnson and L. Peluso, Role of Environmental Deposits and Operating Surface Temperature in Spallation of Air Plasma Sprayed Thermal Barrier Coatings,. Surface and Coatings Technology 86 (1996) 116 -126

[6.] F. Stott, D. Wet and R. Taylor, The Effects of Molten Silicate Deposits in the Stability of the Thermal Barrier Coatings for Turbine Applications at Very high Temperatures. 3rd International SAMPE Metals Conference. (1992)

[7.] J. Dixon and S. Weed , Minerals in Soil Environments. 2nd Edition. Soil Society of American Book Series USA (1989).

[8.] J. Mackenzie and D. Canil, Volatile Heavy Metal Mobility in Silicate Liquids: Implications for Volcanic Degassing and Eruption Prediction, Earth and Planetary Science Letters Volume 269 (2008) 488 – 496.

[9.] S. Kramer, J. Yang and C. Levi, Thermochemical Interaction of Thermal Barrier Coatings with CMAS Deposits, Journal of the American Ceramic Society. Vol 89 [10] (2006) 3167 – 3175.

[10.] K. Grant, S. Kramer, J. Lofvander and C. Levi, CMAS Degradation of Environmental Barrier Coatings,. Surface and Coatings Technology 202. (2007) 653 – 657.

[11.] C. Mercer, S. Faulhaber, A. Evans and R. Darolia, A Delamination Mechanism for the Thermal Barrier Coatings Subject to CMAS Infiltration, Acta Materialia 53 (2005) 1029 – 1039

[12.] S. Kramer, J. Yang and C. Levi, Infiltration-Inhibiting Reaction of Gadolinium Zirconate Thermal Barrier Coatings with CMAS Melts, The American Ceramic Society 91 [2] (2008) 576 – 583.

[13.] C. Chen, Calcium-magnesium-alumina-silicate (CMAS) Delamination Mechanisms in EB-PVD Thermal Barrier Coatings, Surface and Coatings Technology 200. (2006) 3418 - 3427

[14.] S. Kramer, S. Faulhaber, M. Chambers, D. Clarke, C. Levi, J. Hutchingson and A. Evans Mechanisms of Cracking and Delamination within Thick Thermal Barrier Systems in Aero-Engines Subject to CMAS Penetration, Materials Science and Engineering A 490 (2008) 26-35.

[15.] R. G. Wellman and J. R. Nicholls, A Review of the Erosion of TBCs. Journal of Physics D. 40 [16] (2007) 293-305.

Table 1: Table of the samples produced and examined.

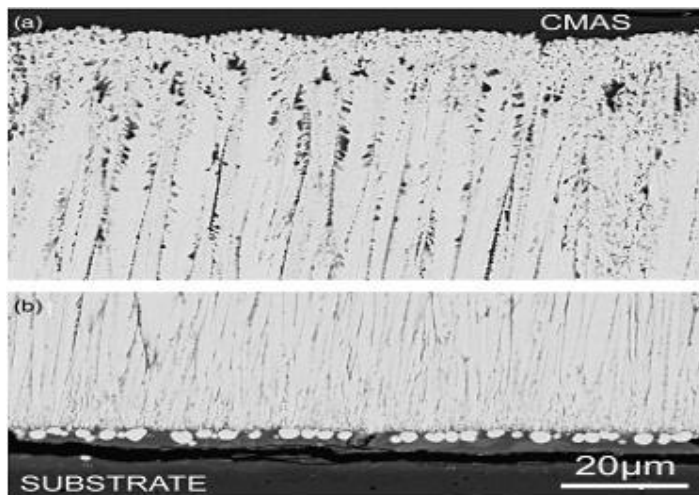Table 2: Elemental EDS analysis of the dark phase in Figure 6a.

Figure 1: (a) Upper Reaction Zone: Bulk CMAS / Column Tips interface showing formation of globular particles. (b) Lower reaction Zone: TBC / Substrate interface. Showing degradation to the substrate [9].
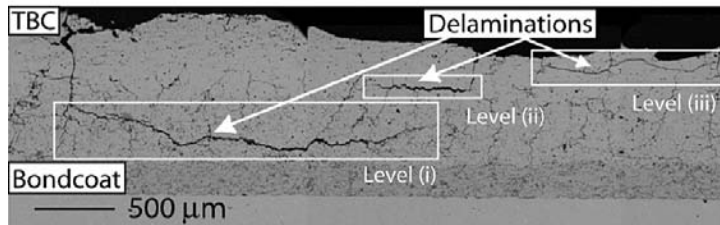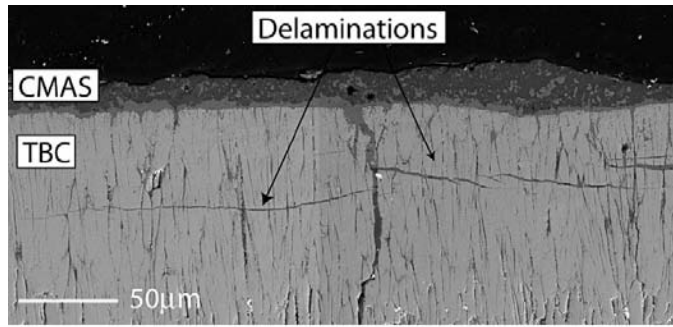
Figure 2: Delaminated TBCs. Top: Sub-surface Mode I delaminations within penetrated zone. Bottom: Delaminations at several locations in shroud. Showing how they always occur from surface connected vertical cracks [13].
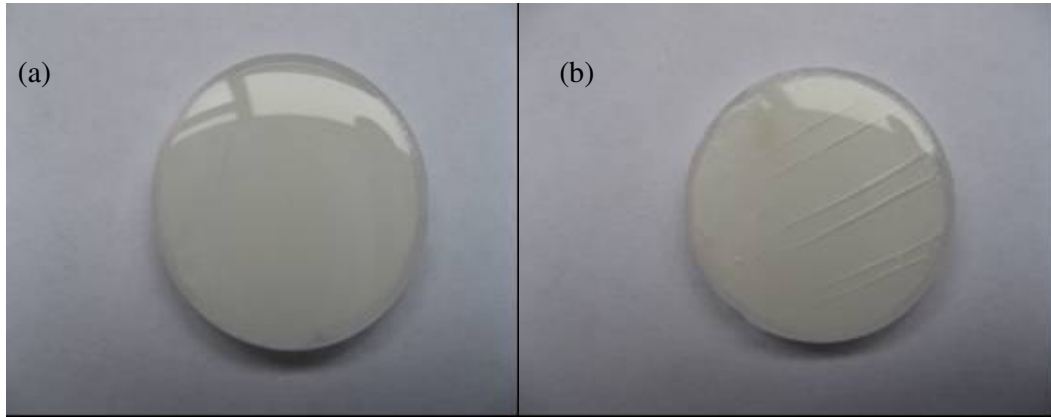
Figure 3: Photos of Samples after heat treatment at 1300°C for 4 hours (a): 'Reacted' CMAS (b) Constituent Powders CMAS, note that in this sample the coating has started to crack.
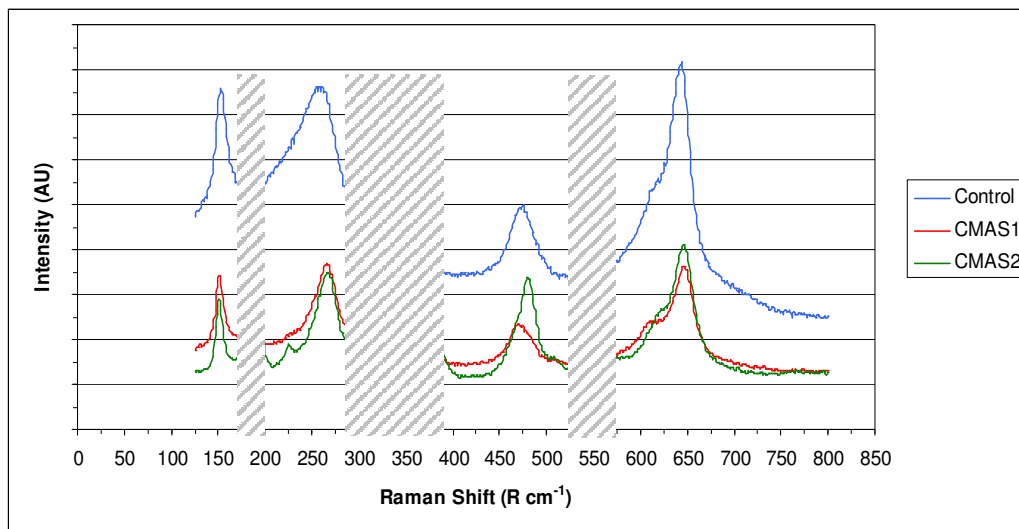
Figure 4: CMAS1, reacted CMAS 120mg/cm^2 and CMAS2, constituent powders 120mg/cm^2 compared to control (no CMAS) using Raman Spectroscopy
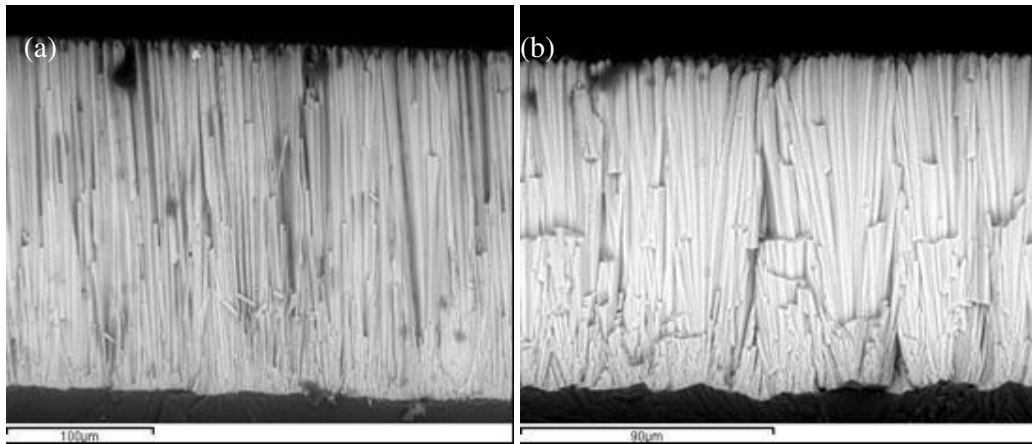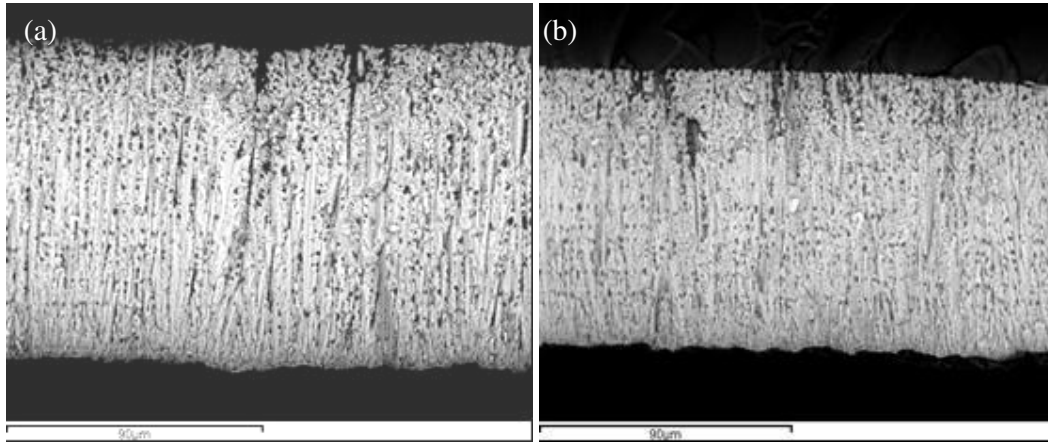
 Figure 5: (a) control (b) Heat treated Control

Figure 6: (a) CMAS 1: Reacted CMAS, (b) CMAS 2: Constituent Powder. The dark phase in both micrographs is where the CMAS has penetrated and then repricipitated.
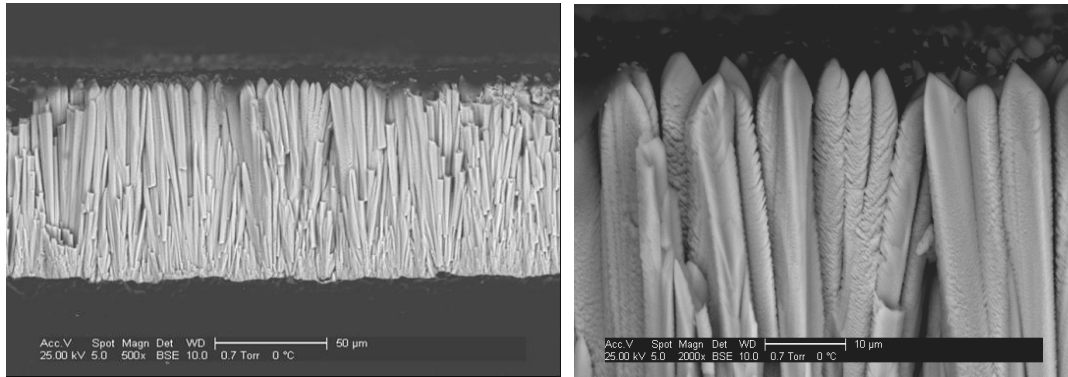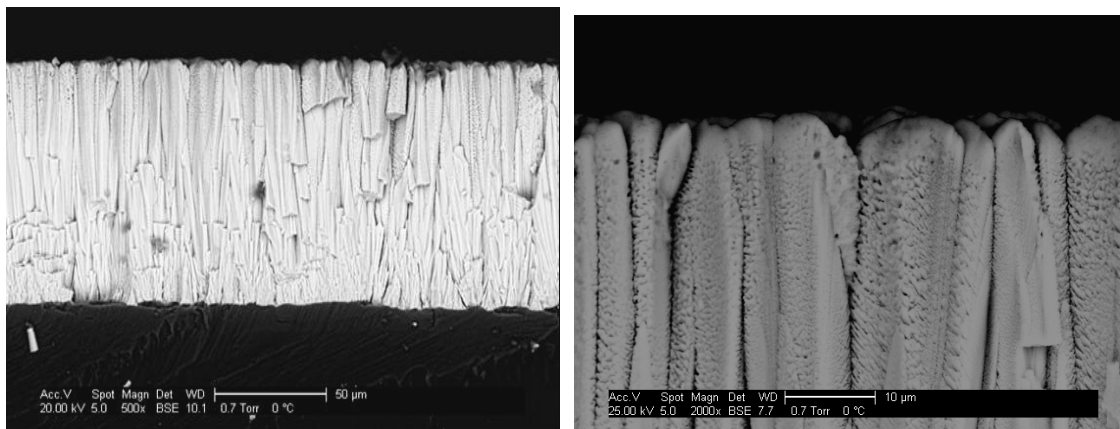
Figure 7: SEM micrograph of a standard EB PVD TBC.

Figure 8: Sample P_0.0075 (1.8mg/cm^2 of constituent powders) after 4hrs at 1300°C for 4

Figure 9: Sample P-0.01g ((2.4mg/cm^2 of constituent powders) after heat treatment at 1300°C for 4hrs, regions of a) CMAS attack and b) no attack.

Figure 10: Sample P_0.02 (4.8mg/cm^2 of constituent powders) after heat treatment at 1300°C for 4hrs, showing significant CMAS penetration.

Figure 11: Top view of sample P_0.02 (4.8mg/cm^2 of constituent powders) after heat treatment at 1300°C for 4hrs, showing CMAS attack on the top of the coating.

Figure 12: Top view of the control sample.

Figure 13: Erosion Curves for the CMAS degraded samples and the control sample.

Figure 14: Graph showing steady state (SS) erosion rate (E) and initial erosion rate.

Figure 15: SEM micrographs of a) the edge of the erosion scar of the CMAS infiltrated sample and b) the centre of the erosion scar of the control sample.

Figure 16: (a) Upper Reaction Zone: Bulk CMAS / Column Tips interface showing formation of globular particles. (b) Lower reaction Zone: TBC / Substrate interface. Showing degradation to the substrate [9].

Figure 17: Delaminated TBCs. Top: Sub-surface Mode I delaminations within penetrated zone. Bottom: Delaminations at several locations in shroud. Showing how they always occur from surface connected vertical cracks [13].

Figure 18: Photos of Samples after heat treatment at 1300°C for 4 hours (a): 'Reacted' CMAS (b) Constituent Powders CMAS, note that in this sample the coating has started to crack.

Figure 19: CMAS1, reacted CMAS 120mg/cm^2 and CMAS2, constituent powders 120mg/cm^2 compared to control (no CMAS) using Raman Spectroscopy

Figure 20: (a) control (b) Heat treated Control

Figure 21: (a) CMAS 1: Reacted CMAS, (b) CMAS 2: Constituent Powder. The dark phase in both micrographs is where the CMAS has penetrated and then repricipitated.

Figure 22: SEM micrograph of a standard EB PVD TBC.

Figure 23: Sample P_0.0075 (1.8mg/cm^2 of constituent powders) after 4hrs at 1300°C for 4
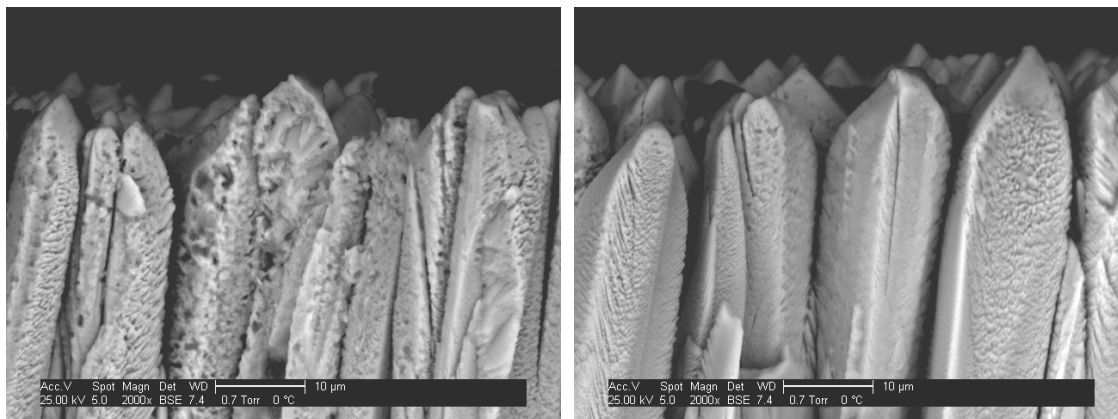
a)   b)

Figure 24: Sample P-0.01g ((2.4mg/cm^2 of constituent powders) after heat treatment at 1300°C for 4hrs, regions of a) CMAS attack and b) no attack.

10 µm   10 µm
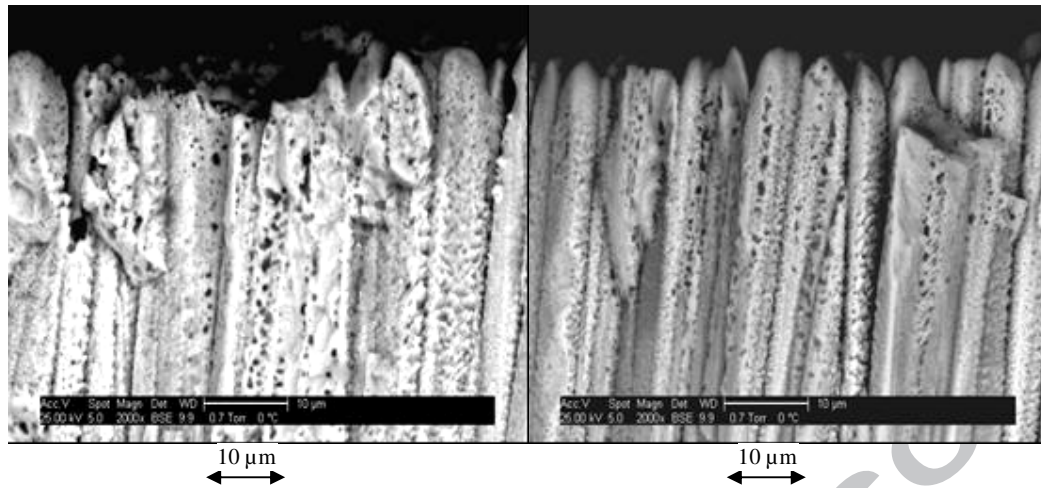
Figure 25: Sample P_0.02 (4.8mg/cm^2 of constituent powders) after heat treatment at 1300°C for 4hrs, showing significant CMAS penetration.
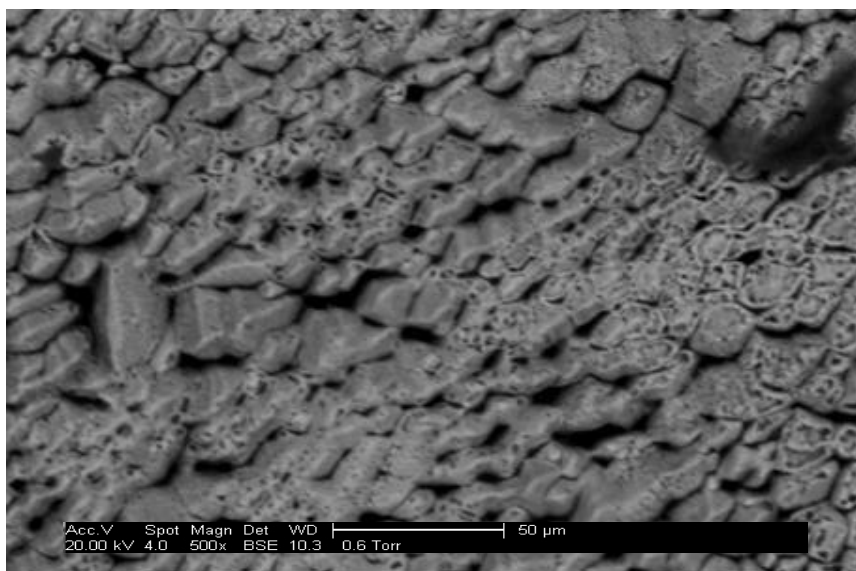
Figure 26: Top view of sample P_0.02 (4.8mg/cm^2 of constituent powders) after heat treatment at 1300°C for 4hrs, showing CMAS attack on the top of the coating.
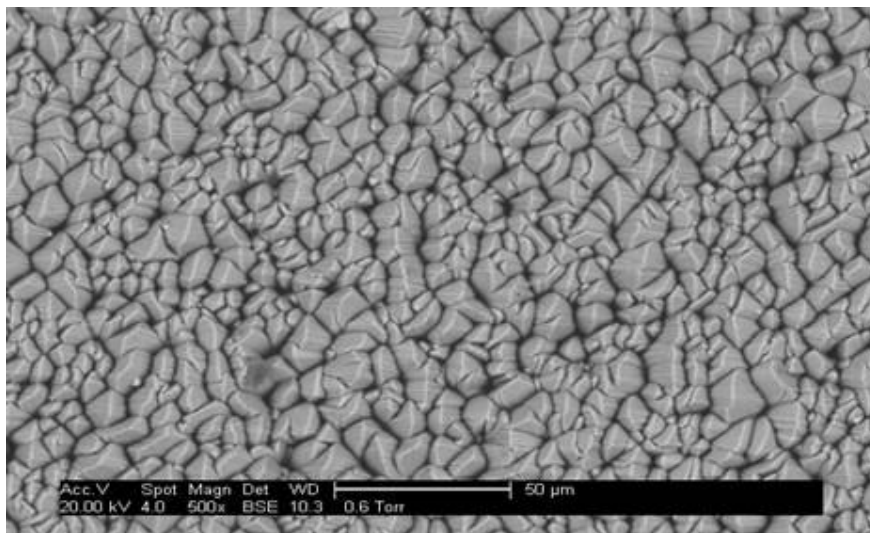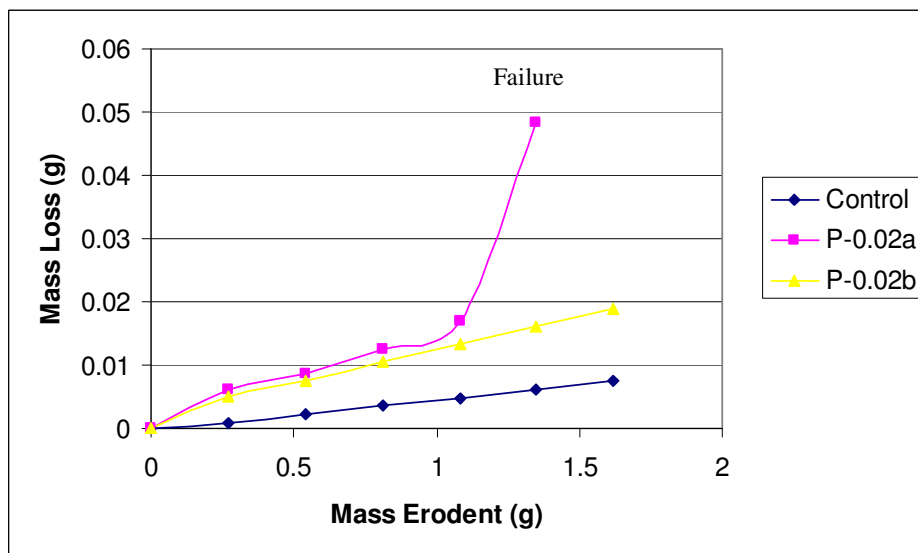
Figure 27: Top view of the control sample.

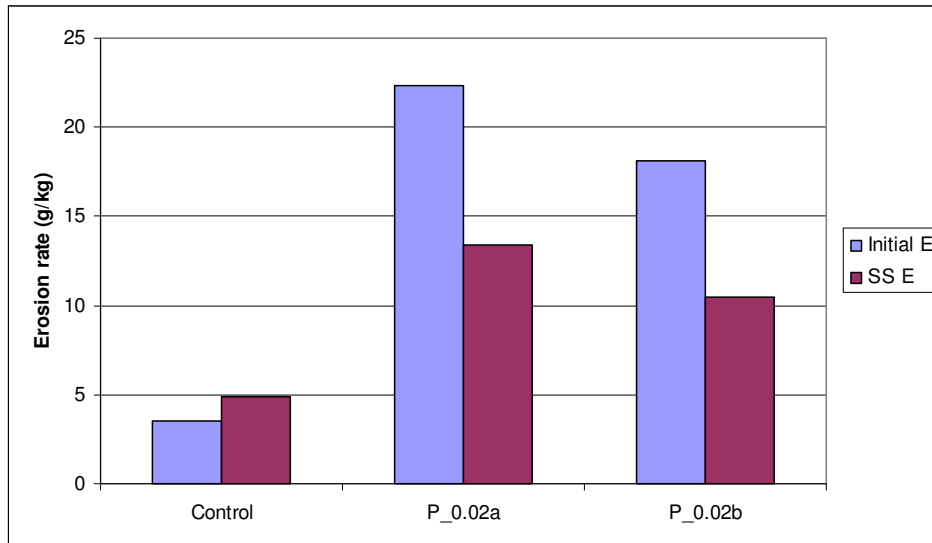Figure 28: Erosion Curves for the CMAS degraded samples and the control sample.

Figure 29: Graph showing steady state (SS) erosion rate (E) and initial erosion rate.
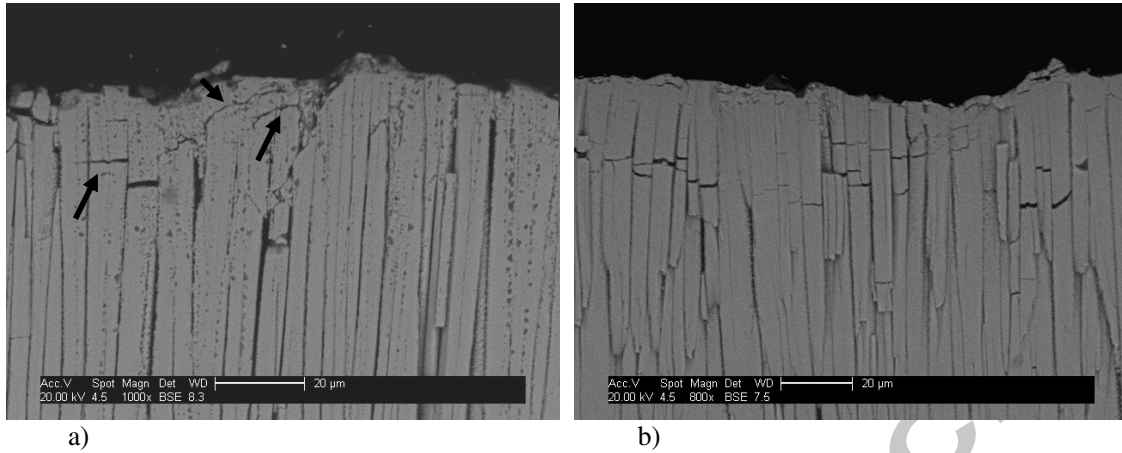
Figure 30: SEM micrographs of a) the edge of the erosion scar of the CMAS infiltrated sample and b) the centre of the erosion scar of the control sample.

Sample	CMAS Type	Mass CMAS (g)	Mass/Area (mg/cm^2)	Time at Temperature
CMAS 1	Reacted CMAS	0.5	120	4hrs at 1300°C
CMAS 2	Constituent Powders	0.5	120	4hrs at 1300°C
P_0.0075	Constituent Powders	0.0075	1.8	4hrs at 1300°C
P_0.01	Constituent Powders	0.01	2.4	4hrs at 1300°C
P_0.0125	Constituent Powders	0.0125	3.0	4hrs at 1300°C
P_0.02	Constituent Powders	0.02	4.8	4hrs at 1300°C
P_0.03	Constituent Powders	0.03	7.2	4hrs at 1300°C

Table 3: Table of the samples produced and examined.

Element	Weight %
O	45.8
Mg	0.8
Al	13.9
Si	5.2
Ca	5.1
Y	0.8
Zr	27.7
Hf	0.8

Table 4: Elemental EDS analysis of the dark phase in Figure 6a.

CMAS corrosion of EB PVD TBCs: Identifying the minimum level to initiate damage

Wellman, R. G.

2010-01-01T00:00:00Z